A&A 378, 153–164 (2001)
DOI: 10.1051/0004-6361:20011174

Astronomy & Astrophysics

Surface abundance distribution models of Si, Cr, Mn, Fe, Pr and Nd for the slowly rotating Ap star HD 187474⋆

S. Strasser[1], J. D. Landstreet[1], and G. Mathys[2]

[1] University of Western Ontario, Department of Physics & Astronomy, London, Ontario, N6A 3K7 Canada
[2] European Southern Observatory, Casilla 19001, Santiago 19, Chile
e-mail: gmathys@eso.org

Received 5 March 2001 / Accepted 21 August 2001

Abstract. The very slowly rotating magnetic Ap star HD 187474 has strong and quite variable spectral lines of several elements. An axisymmetric low-order multipole magnetic model has been obtained for this star by Landstreet & Mathys (2000). HD 187474 is one of the few very slowly rotating magnetic Ap stars that is suitable for abundance distribution modelling; because of the unusually large angle between the field and rotation axes, the line of sight goes well into both magnetic hemispheres. We have used CASPEC and CES spectra with good phase coverage together with the programme ZEEMAN to search for simple three-ring abundance distributions of Si, Cr, Mn, Fe, Pr and Nd, symmetric about the assumed magnetic field distribution axis, that match observed line profiles as a function of rotational phase. Reasonably satisfactory fits to the observations are found for all of these elements. In all cases, three-ring models work as well as more finely gridded models. The deduced abundances are somewhat overabundant and somewhat non-uniform for Fe; for the other elements quite large overabundances (up to 5 dex for Nd) are found, with substantially higher (but somewhat unequal) abundances around the two magnetic poles compared to the magnetic equator. All the elements studied are overabundant everywhere (except perhaps Si around the magnetic equator). This star poses a real challenge to theories of chemical peculiarity.

Key words. stars: abundances – stars: chemically peculiar – stars: magnetic fields – stars: fundamental properties

1. Introduction

HD 187474 = HR 7552 is a fifth-magnitude A0EuCrSr Ap star. A reversing longitudinal magnetic field B_l, which varies between approximately +2000 and −2000 G, was discovered by Babcock (1958), who eventually concluded that the star has an extraordinarily long rotation period, currently estimated to be 2345 d ≈ 6.4 yr (Mathys 1991). Although a few magnetic Ap stars are known with still longer periods (γ Equ is thought to have a period of the order of 75 yr!), HD 187474 is nevertheless one of the most slowly rotating magnetic Ap stars known. The star is also observed to be a strong spectrum variable; the equivalent widths of lines of Cr, Mn, Fe, Si, Nd, and Pr all vary by factors of order two during the rotation period of the star.

Didelon (1987) discovered that the star shows a number of line profiles that are clearly resolved into Zeeman multiplets by the magnetic field, and showed that the mean field modulus B_s that may be measured from this splitting varies with the stellar rotation period, with a typical value of around 5–6 kG. During the past several years, Mathys (1991), Mathys & Hubrig (1997), and Mathys et al. (1997) have obtained extensive measurements of several magnetic moments of HD 187474, including B_l, B_s, the mean quadratic field B_{mq} (which measures the average over the visible hemisphere $(\langle B^2\rangle + \langle B_z^2\rangle)^{1/2}$), and the crossover field B_{xover} (which measures $v \sin i \langle x B_z\rangle$, where x is the normalized distance from the stellar rotation axis in the plane of the sky and $v \sin i$ is the projected rotation velocity of the star).

The magnetic field of this star has been modelled by Landstreet & Mathys (2000) as a sum of centred, colinear dipole, quadrupole, and octupole fields of polar strength $B_d = -7700$ G, $B_q = -1600$ G, and $B_o = 1000$ G; the local magnetic field is thus about 50% stronger at the negative magnetic pole than at the positive pole. The axis of symmetry of the model magnetic field is inclined to the stellar rotation axis at an angle of $\beta = 45°$, and the rotation axis makes an angle of $i = 87°$ with the line of sight. As shown by Landstreet & Mathys, this model reproduces the available magnetic field observations of the star quite accurately. Furthermore, because both angles i and β are relatively large, so that the star is viewed from about 45° above the magnetic equator to about 45° below the

Send offprint requests to: J. D. Landstreet,
e-mail: jlandstr@uwo.ca

⋆ Based on observations collected at the European Southern Observatory, La Silla, Chile.

equator, the magnetic model is rather well constrained; the uncertainty of the model parameters is of the order of 10% of the parameter values. This relatively favorable geometry is *not* generally found among the magnetic Ap stars of long period; most have an inclination angle β between the magnetic and rotation axes of only 10 or 20°. HD 187474 is one of the very few long-period magnetic Ap stars for which a model with reasonably well-constrained parameters can be derived. It is thus particularly well-suited for modelling.

Although the star is a striking spectrum variable, no effort has previously been made to determine the average element abundances of this star, to model the variations of abundance over the stellar surface, or to explore whether the spectral line profiles contain further information about the magnetic field distribution beyond that revealed by the field moment measurements. Such modelling is certainly of interest, and in fact is a major direction of current work by several groups with expertise in Zeeman Doppler imaging. However, HD 187474 is not a particularly suitable star for Zeeman Doppler imaging, mainly because the rotation period is so long that the spectral lines are essentially unbroadened by rotation (the equatorial rotational velocity is approximately 0.1 km s^{-1}). There is thus no information about the longitudinal variations of the field or abundance encoded by rotational Doppler shifts in various parts of the spectral line profiles. The only such information is in the time variations of the disk-integrated line profiles. Since this situation means that much less information is available than is normally needed even to produce a low resolution map of field or abundance structure, HD 187474 probably cannot be mapped in detail by Zeeman-Doppler imaging, at least in the near future.

Nevertheless, from synthesis of the strengths and profiles of spectral lines as a function of rotational phase it should be possible to infer a simple model of the abundance distributions of several elements. From such modelling we could hope at least to get some idea of the average abundances of a few elements, and some estimate of the scale of their variation over the stellar surface. Furthermore, with such a model we could test to some extent the correctness of the magnetic field geometry that has been derived from field moments. We have therefore carried out modelling of a number of spectral lines in HD 187474. This paper discusses the results – and limitations – of this project. In the following section, we describe the observational material used for this project; in Sect. 3 we discuss the modelling techniques employed; Sect. 4 describes the results obtained; and the work is summarized in Sect. 5.

2. Observations

The data available for analysis include 10 intensity spectra taken with the Coude Auxiliary Telescope (CAT) and the Coude Echelle Spectrograph (CES) of the 3.6-m telescope at the European Southern Observatory, originally obtained for measurements of B_s, and 18 circularly analyzed spectra obtained with the Cassegrain Echelle Spectrograph (CASPEC) on the 3.6-m telescope, originally obtained for measurements of B_l, B_{mq}, and B_{xover}. Rotational phases of these data have been computed with the ephemeris of Mathys (1991), on which phase 0.0 coincides with the positive extremum of B_l. The CES spectra (except for the one at phase 0.86) cover a spectral range of about 50 Å between 6122 and 6175 Å. They were obtained at a resolving power of 100 000, and (except for one spectrum, at phase 0.53) have a signal-to-noise ratio in the range 90–150. The CES spectra used are listed in Table 1.

The CASPEC data used are listed in Table 2. These spectra fall into two groups. One set, obtained between 1985 and 1988, were obtained with a resolving power of about 15 000 and have signal-to-noise ratios near 100. These are the unfortunately the only CASPEC data available for phases from 0.75 to 0.25. These spectra cover most of the spectral window between 5730 and 6730 Å. The second set, which fall in the phase interval 0.30 to 0.75, were obtained between 1995 and 1997. They have a resolution of about 40 000, have signal-to-noise ratios near 150, and span a slightly larger wavelength window than the older spectra.

Both of the data sets have relatively complete phase coverage. The largest phase gaps are about 0.15 long in phase. Considering the phase coverage and the resolving power of the data, and keeping in mind that our goal here is primarily a first estimate of chemical abundance distributions in this star, we have mainly concentrated on the series of ten CES spectra, which are spaced pretty uniformly through the rotation cycle. Abundance models are derived from these data for Cr, Fe, Nd and Pr, all of which have unblended lines in the small window. The nine CASPEC spectra were used to derive abundance models for Si, an important element for which no lines are available in the CES spectra, and Mn, for which one or two unblended lines are also available in most of the CES spectra.

Table 1. High-resolution (CAT-CES) spectra.

JD	Phase	S/N	Window (Å)
2449214.805	0.044	150	6123–6175
2449535.851	0.181	120	6123–6175
2449882.916	0.329	120	6126–6178
2450162.911	0.449	120	6124–6176
2450356.519	0.531	50	6123–6175
2450522.904	0.602	90	6123–6175
2450702.569	0.679	100	6123–6175
2450900.908	0.763	140	6122–6177
2448788.856	0.863	110	6141–6167
2449100.889	0.996	100	6125–6178

HD 187474 is a spectroscopic binary with a period of 690 days (Leeman 1964). The secondary is not visible in our spectra. All the spectra were shifted to zero radial velocity by adding the necessary Doppler shift with IRAF.

Table 2. Low-resolution (CASPEC) spectra.

JD	Phase	S/N	Window (Å)
2446894.874	0.055	100	5730–6727
2447280.834	0.220	100	5730–6732
2449830.905	0.307	150	5532–6799
2450039.524	0.396	150	5533–6799
2450294.827	0.505	150	5530–6796
2450505.908	0.595	150	5530–6795
2450783.513	0.713	150	5529–6796
2446218.864	0.767	100	5710–6714
2446547.865	0.907	100	5640–6710

3. Modelling technique

Our model is obtained using one of the versions of the Fortran programme ZEEMAN described by Landstreet (1987), Landstreet et al. (1988), and Wade et al. (2001). ZEEMAN is a programme that synthesizes the spectral lines in one or several small wavelength windows at a number of rotational phases, compares the resulting spectrum with observed spectra at those phases, and tries to optimize a simple parameterized abundance distribution to achieve the best possible agreement with the observed spectrum. For abundance modelling, the programme assumes a simple axisymmetric magnetic field distribution described by a low-order multipole expansion (dipole, quadrupole, and linear octupole). The abundance distribution is assumed to be axisymmetric about the magnetic axis, and is described as a series of up to six rings of equal extent in colatitude, on each of which the abundance is uniform. The abundance on each ring is varied by the programme as it searches for a best fit to the observed spectra. Up to three wavelength windows may be fit simultaneously, and blends may be included iteratively, although the programme only tries to optimize the abundance distribution of one element at a time. The effect of the magnetic field on spectral line profiles is fully taken into account; the coupled equations of transfer for the four Stokes parameters are solved simultaneously, including anomalous dispersion.

The effective temperature and gravity were assumed to have the values $T_{\rm e} = 10\,400$ K (Glagolevskij 1994) and $\log g = 4.0$ (which are consistent with the values $T_{\rm e} = 10\,100 \pm 300$ K and $\log g = 3.94 \pm 0.09$ recently determined by Hubrig et al. 2000). The microturbulence velocity parameter was taken to be zero. Due to the very slow rotation of HD 187474, $v \sin i$ was kept fixed at 0 $\mathrm{km\,s^{-1}}$. The magnetic field geometry assumed was that found by Landstreet & Mathys (2000), as described in the Introduction. With this geometry, we observe the magnetic field up to about 45° from each pole during the rotation cycle of the star. The weaker, positive pole is closest to the line of sight at phase 0.

In general, atomic data were taken from Moore (1952, 1959), Martin et al. (1978, 1988), and the Vienna Atomic Line Database (Piskunov et al. 1995; Ryabchikova et al. 1999; Kupka et al. 1999). There were a few lines which did not seem to be blended, and for which all relevant atomic data was available, but for which the calculated profile was much stronger or weaker than the observed one. We modelled such discordant lines in available spectra of the weakly magnetic Ap stars HD 8441 and HD 22374 to investigate the possibility of erroneous gf values (see Sect. 4 for details). The lines used for abundance modelling are listed in Tables 3 and 4, where we include adopted values of a few necessary atomic parameters which were either unpublished or appeared to be incorrect.

Table 3. Spectral lines modelled with CES spectra.

Line	Wavelength	Comment*
Cr II	6134.465	$\log gf = -2.26$ assumed
Cr II	6138.721	
Cr II	6147.154	
Cr II	6150.543	unidentified blend; rejected
Cr II	6157.832	blend with Nd II
Cr II	6158.108	blend with O I
Cr II	6158.181	blend with O I
Cr II	6158.621	possibly unrecognized blend
Cr II	6161.031	blend with Pr II & III
Cr II	6168.520	unidentified blend; rejected
Fe I	6136.620	very weak
Fe I	6137.692	very weak
Fe II	6147.741	
Fe II	6149.260	
Nd II	6133.452	
Nd III	6145.070	$g_{\rm l} = 1.070$; $g_{\rm u} = 1.054$
Nd II	6157.822	blend with Cr II
Nd II	6166.651	
O I	6155.9	
O I	6156.7	
O I	6158.2	blend with Cr II
Pr III	6160.244	$g_{\rm l} = 0.966$; $g_{\rm u} = 1.002$
Pr II	6161.179	blend with Cr II & Pr III
Pr III	6161.224	blend with Cr II & Pr II; $g_{\rm l} = 1.098$; $g_{\rm u} = 0.973$
Pr II	6165.891	
Si I	6142.204	
Si I	6142.483	
Si I	6155.134	

The process of finding the best abundance distributions of the various elements basically consisted of finding an unambiguous model that is able to reproduce the varying profiles of the least blended spectral lines. As previously explained, our programme varies the abundances of one element at a time on up to six rings axisymmetric about the magnetic axis. We investigated models with between two and six rings. The first step was to determine which spectral lines are suitable for modelling. Initially, each line was modelled by itself to give us a rough estimate of the abundance to be expected. This was done for models

Table 4. Spectral lines modelled with CASPEC spectra.

Element	Wavelength	Element	Wavelength
Fe II	5952.510	Nd II	5804.004
Fe II	6175.146	Nd II	5865.027
Fe II	6175.455	Nd II	5900.406
Fe II	6416.919	Nd II	6591.430
Mn II	5752.231	Pr II	5892.251
Mn II	5963.277	Pr II	6429.629
Mn II	6122.450		
Mn II	6122.829	Si II	5957.559
Mn II	6123.193	Si II	6347.109
Mn II	6123.418	Si II	6371.371
Mn II	6125.225		
Mn II	6125.533		
Mn II	6125.861		
Mn II	6130.801		
Mn II	6130.917		
Mn II	6131.041		

from two to six rings. We then grouped together the best lines (lines which appeared to be unblended, which gave roughly concordant abundance maps, and for which the Zeeman pattern assumed seemed to describe the line splitting reasonably well) of differing equivalent widths for Si, Cr, Mn and Fe, the four elements for which more than one line suitable for mapping was available, and searched for abundance distributions which reproduced all lines of one element simultaneously for all modelled phases. Different combinations of both two and three lines were explored in this step, but it was sufficient to use the abundance distribution found from two lines to fit the other lines (the quality of the fits was not improved by going to various combinations of three lines).

We started the modelling of two or three lines at once with a three ring model with all the rings varying. The next step then was to increase the number of rings to see if the lines could be fit better. We investigated four varying rings; five rings with all five varying, or keeping one polar cap fixed; and six rings keeping one polar cap fixed. None of the distributions with four or more rings showed any obvious improvement over models using only three rings (see Sect. 4 for details). The failure of models with more rings to approximate better the observed line profiles may be due to unrecognized blends, to vertical stratification, to magnetic splitting not correctly described by the assumed field structure, or to abundance variations with magnetic longitude which are ignored in this simple chemical distribution model.

In principle, we should have been able to find better distribution models by modelling all the "good" lines of a single element simultaneously, particularly for Cr, Mn and Fe. We chose instead to determine our best fit models normally using only one or two lines. There were two reasons for this. The first is a practical one; ZEEMAN is at present not equipped to do the bookkeeping for more than three line regions at once, and it is unable to fit simultaneously two dissimilar groups of spectra (such as one set of CASPEC and one set of CES spectra). Furthermore, in this star even the good lines often appear to be mildly blended. We preferred to use only the cleanest lines, and the best available resolving power, for finding our best fit models. In most cases we had one or two lines that appeared to satisfy these criteria better than any of the others.

4. Results

4.1. Silicon distribution

There are no detectable Si II lines in the high-resolution window. However, there are five strong Si II lines in the CASPEC data, of which three turned out to be suitable for modelling (good atomic data, little apparent blending, not close to order edges). We used the λ 5957 and the λ 6371 lines together to derive the final Si model. Both of these lines, as well as the λ 6347 line, are reasonably well fit at most phases, as can be seen in Fig. 1. However, for each line there is one phase at which the model fit is relatively poor. This discordance occurs at phase 0.713 for the λ 5957 line and phase 0.505 for the λ 6347 and λ 6371 lines. Using more rings did not solve this problem, and no other combination of lines led to any better model than the one adopted.

The abundances $\log \epsilon_{\rm Si} = \log(n_{\rm Si}/n_{\rm H})$ for each ring of the best model found are listed in Table 5, in which ring co-latitude is measured from the stronger negative pole, visible around phase 0.5. The adopted model has very high Si abundances at the poles and a much lower abundance in the middle ring. This character is consistent with the

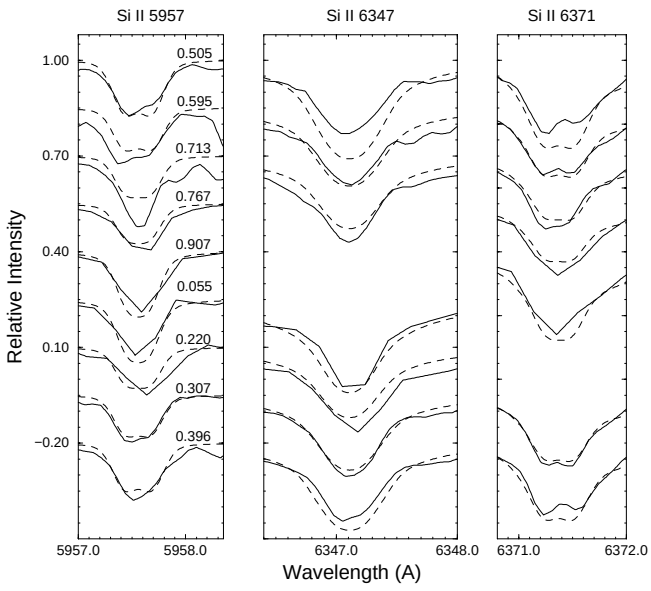

Fig. 1. A plot showing the three-ring fits to the observed profiles of three lines of Si II. Observations are shown as solid lines; model fits are dashed. Successive phases are separated by 0.15 in intensity. The phases are labeled inside the left panel.

Table 5. Abundance distributions.

	$\mathrm{Log}(n_\mathrm{A}/n_\mathrm{H})$						
Ring	O	Si	Cr	Mn	Fe	Pr	Nd
0–60° (negative pole)	−3.64	−3.02	−4.43	−4.10	−3.17	−6.65	−6.64
60–120° (magnetic equator)	−3.97	−6.50	−4.37	−6.21	−4.12	−9.30	−9.00
120–180° (positive pole)	−3.88	−2.69	−3.74	−3.30	−3.22	−5.49	−4.94
χ^2/ν of fit to selected lines	1.4	11.2	3.0	3.4	12.7	4.1	7.1
Best fitting uniform abundance	−3.83	−4.30	−4.18	−4.38	−3.61	−7.45	−7.56
χ^2/ν of uniform fit	1.4	33.5	7.0	5.3	17.3	24.0	37.2
Solar abundance	−3.17	−4.45	−6.33	−6.61	−4.50	−11.29	−10.50
χ^2/ν of solar fit	65.5	40.9	109	17.3	184	259	188

variations of the Si lines, which are stronger around phases of magnetic pole passage (near phases 0.0 and 0.5) and weaker near the magnetic equator (phases 0.25 and 0.75), but the abundance contrast selected by the programme is surprisingly large. Going to a four ring model did not soften the contrast.

To provide a quantitative indication of how successful our best fit model is, we list in the table, below the abundances on the three rings, the χ^2/ν of the fit to the spectral lines used to find the best fit. This value is only roughly indicative. It assumes that all the spectra had the same signal-to-noise ratio of 120, and it is computed over windows which include only the spectral lines synthesized. Consistent with Fig. 1, the value of χ^2/ν of the fit indicates that our simple model is (mostly) able to fit the general character and variations of the Si II lines, but certainly cannot fit them to the precision of the data. The discrepancy between the model and the observed lines of Si is typically around 3% of the continuum.

The uncertainties in the abundances listed in Table 5 are somewhat difficult to quantify. The fitting programme normally finds several different abundance distributions that fit the observations almost equally well; these typically vary in abundance on a particular ring by 0.1 or 0.2 dex. However, when we use a different number of rings for modelling, the deduced abundances may change by 1 dex or even more. Since the model abundances represent some kind of average over large regions of a star on which abundances certainly vary by some dex from one point to another, it is not surprising that averaging over different regions leads to rather different model abundances. However, this does mean that we cannot easily specify the uncertainties of our models.

One way of exploring the uncertainties in the model abundances without mapping the whole parameter space of the three abundance parameters (the abundances on the three rings) is to look at some representative cuts through the χ^2/ν surface for simple parameter variations. Three such cuts are shown for Si in Fig. 2. In the left panel, we hold the abundance of Si on the equatorial ring constant at $\log\epsilon_\mathrm{Si}(\mathrm{eq}) = -6.50$ (open circles; the equatorial ring abundance of the best fitting model) or −4.45 (filled circles; the solar value). The abundances at the two poles are varied by $\Delta\log\epsilon$ around $\log\epsilon_\mathrm{Si}(\mathrm{neg\,pole}) = -3.00$ and $\log\epsilon_\mathrm{Si}(\mathrm{pos\,pol}) = -2.70$. It is clear from the figure that reducing the abundances at both poles by about one dex from the value in Table 5 leads to a substantially worse fit than the best model obtained, and that the abundances at the poles can hardly be increased by more than about 0.5 dex. Furthermore, no model with the adopted abundance difference between the two poles and a solar abundance of Si at the equator gives an acceptable fit.

In the right panel of Fig. 2, we hold the abundances on the two polar rings constant at the values given for the best fit to Si in Table 5. The variation of χ^2/ν as the abundance on the equatorial ring is varied around $\log\epsilon_\mathrm{Si}(\mathrm{eq}) = -6.50$ (open circles) shows that in fact to obtain an acceptable model the abundance on the equatorial ring simply needs be small enough (less than about −5.5) to make the contribution to the disk-integrated line from this ring negligeable; for larger values than this, the value of χ^2/ν increases rapidly to unacceptable values. Thus the abundance reported for the equatorial ring is simply the largest value for which this ring contributes almost nothing to the integrated line; the abundance could be somewhat larger, or quite a lot smaller, than the reported value.

Another interesting kind of information is a measure of how much better our three-ring models fit the observations compared to a *uniform* distribution (abundance value the same on all three rings). This provides information about whether the large contrasts in abundance that we find for Si (and other elements) are actually required to reproduce the spectra. To explore this question, we have run two further kinds of fits. Information about these fits is also shown in Table 5.

First, we have used the same spectral lines as before to search for the best fitting uniform abundance. Both the best uniform abundance and the value of χ^2/ν of this fit, computed as for the three-ring model, are shown in the table below the data for the three-ring model. In the case of Si, the value of the $\chi^2/\nu = 33.5$ of the fit of a uniform

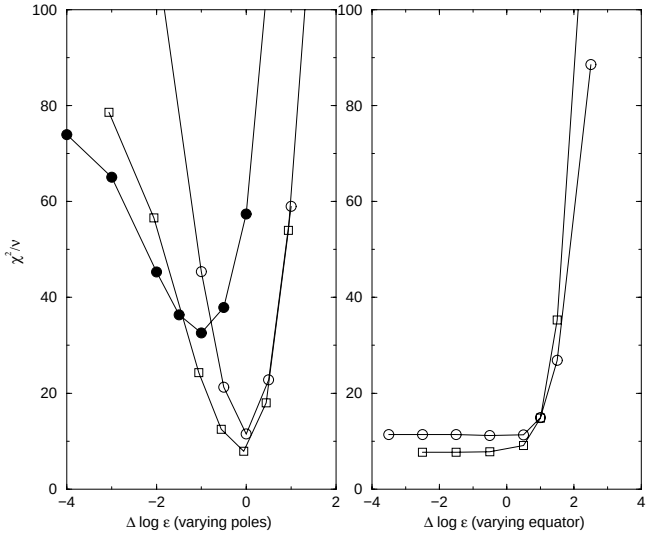

Fig. 2. Representative cuts through the χ^2/ν surface. In the left panel, the abundance at the magnetic equator is held constant while the abundances on the two polar rings are varied together. In the right panel, the abundance at both poles is held constant while the abundance on the equatorial ring is varied. Dots and open circles refer to the distribution of Si, open squares to the abundance of Nd. The details of the figure are discussed in the text.

distribution of Si to the observations is considerably worse than that found for our best three-ring model (11.2); the uniform fit does not appear to constitute an acceptable alternative to our high-contrast model.

Secondly, to show that this star has abundances which are mostly far from solar, we have computed the value of χ^2/ν for the fit to the same spectral lines assuming uniform solar abundances (Grevesse & Sauval 1998) for all elements. The value of χ^2/ν for this fit is reported in the last line of Table 5. In all these computations the same magnetic model is assumed. Clearly, in the case of Si, a uniform solar abundance model, for which the equivalent widths are typically more than a factor of two smaller than the observed lines, is completely unacceptable.

We conclude that it is not possible to fit the Si II variations in this star without using a model that has at least 2 dex higher abundance at the poles than at the equator, and that the abundance of Si near the poles must be at least 1 dex higher than the solar value, while that near the equator must be about 1 or more dex below solar.

There are two unblended Si I features in the wavelength window of the CES spectra that are suitable for modelling. These are listed in Table 3. They are not visible in the stellar spectra, but when we computed their strengths using the abundance model derived from Si II lines in the CASPEC spectra, we found that both lines are predicted to be visible at some phases. The line at 6155 Å presents the strongest discrepancy with the observed spectra; it is expected to be slightly deeper than observed between phases 0.329 and 0.763, but for phases around 0.5 the predicted line is substantially stronger (about 0.15 of the continuum level deep) than observed. This appears to represent a significant discrepancy between lines of the two ionization states, and may be evidence for vertical stratification of this ion. However, the discrepancy could also be due to an error in the assumed effective temperature or gravity, or could be the effect of a small departure from LTE. Furthermore, the lines of Si II on which the model is based are saturated, so small errors in fitting them can lead to significant abundance errors. As a result, the interpretation of the discrepancy is not very clear. The concordance between lines of different ion states is a question that certainly deserves further investigation.

4.2. Chromium distribution

In modelling Cr, we tried a number of configurations for the rings. The models with more rings were not significantly better than the models with three rings. The final model was obtained from the best simultaneous fit to the λ 6138 and the λ 6147 lines. Both of these lines are well fit by the model. The adopted model also fits reasonably well five closely adjacent lines at λ 6158, but the quality of the fit is significantly worse than for $\lambda\lambda$ 6138 and 6147. The poorer fit to λ 6158 might be due to the modelling assumption of axial symmetry, or to unrecognized blends. We found that the $\log gf$-value for the λ 6134 line given by VALD was incompatible with the observed lines in HD 187474 as well as in HD 8441 and HD 22374. By changing the value from -3.26 to -2.26 we were able to fit this line well in the latter two stars, and we therefore used this value in our modelling of HD 187474. With the adjusted gf value this line is well fit by the same abundance model as the other Cr lines. Note that the magnetic broadening of this line is pretty well predicted by our model, supporting the view that this feature is indeed due to Cr II. The Cr II line at λ 6150 was rejected for our modelling because for any reasonable abundance distribution the fit was much shallower than the observed line, although comparisons with other stars indicated that the gf value used was approximately correct. The chromium line at λ 6168 also seems to be seriously blended and was not fit well by our model, so it too was rejected. The final fits to the accepted lines are shown in Fig. 3, and the adopted abundances $\log n_{\rm Cr}/n_{\rm H}$ on the three rings of the model are given in Table 5.

We see from Table 5 that Cr is almost constant over the first two rings, but that the abundance rises slightly near the positive pole. This result is confirmed by the equivalent width variation of the lines as a function of phase: the equivalent width is clearly the largest around phase 0.0 (when the positive pole points towards us).

For the lines of Cr, the value of the χ^2/ν of the best fit is substantially better than that reported for Si. This is probably due to several causes: (1) we have a larger choice of lines, from which we have picked those that model best; (2) the lines modelled are in the (higher-resolution) CES spectra; (3) there are no really discrepant phases,

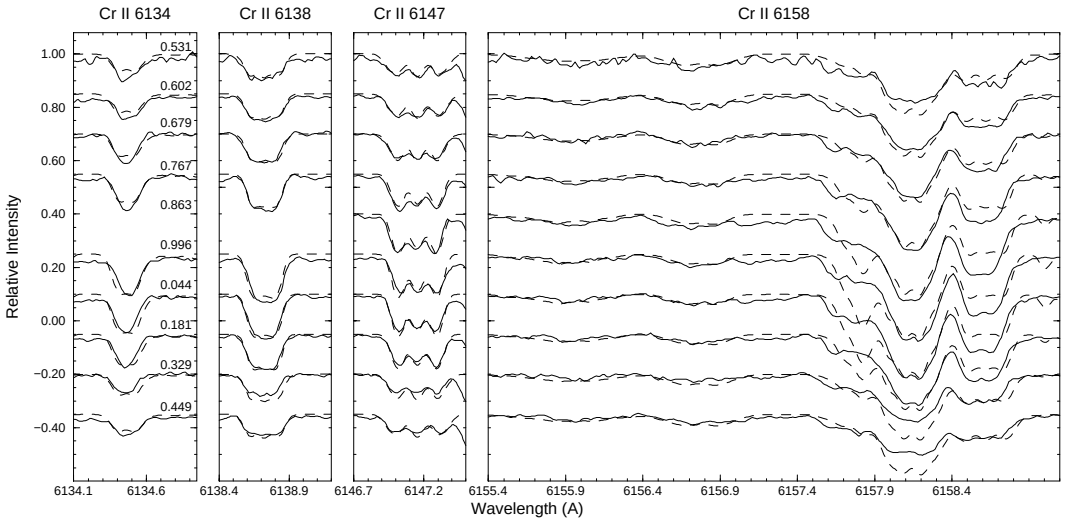

Fig. 3. A plot showing the three-ring fits to the observed profiles of four windows (seven lines) of Cr II. Observations are shown as solid lines; model fits are dashed. Successive phases are separated by 0.15 in intensity. The phases are labeled in the left-hand box. The right-hand panel is quite wide to show the fits to the weak O I lines at 6155.9 and 6156.7 Å, as well as to the Cr II lines (weakly blended with O I) at 6158 Å.

probably because the overall abundance distribution of Cr is not very far from uniform; and (4) the Cr lines are weaker than the Si lines modelled, which means that a given percentage error in the fit results in a smaller value of χ^2/ν than would be found for deeper lines.

For Cr we also report in Table 5 the quality of the best fitting uniform distribution, and of a uniform solar distribution. Although the values of χ^2/ν for the best uniform fit is reasonably small, it is still substantially higher than the best fitting three-ring model found, and we believe that an abundance contrast for Cr of about 0.5 dex between the region around the positive pole and the rest of the star is detected with reasonable confidence. Furthermore, there is no doubt at all that the typical abundance of Cr in HD 187474 is some two dex higher than solar; the lines we have modelled are almost undetectable in spectra of stars of this temperature that have approximately solar abundances. This result is reflected in the very large value of χ^2/ν for a fit to the modelled lines with solar abundance.

4.3. Manganese distribution

There are many strong Mn lines in the CASPEC data window, of which several are also in the CES window. Thus a lot of information is available about this ion. However, an important weakness of our analysis is that Mn has substantial hyperfine structure which is not included in our calculations. This introduces a significant uncertainty into the abundances we derive, since most of the CASPEC lines are saturated. Furthermore, almost all the lines we consider between 6122 and 6131 Å come from transitions in which the fine-structure splitting is comparable to the magnetic splitting, so these lines should be treated in the partial Paschen-Back case; again, our programme is not presently able to consider this case. However, the effect of the magnetic field is to desaturate lines in a manner similar to that produced by hyperfine splitting, and the Zeeman approximation to splitting provides at least a first approximation to the behaviour of these lines in a magnetic field. Therefore we have tried to model Mn in the same way as other elements, in order to obtain at least an approximate abundance model of this ion.

We experimented with modelling CASPEC lines in several regions. The model presented here was found by fitting the λ 5752 and the λ 5963 lines together. These two lines are not very different in depth, but the model found with these lines fit the other lines better than models found from other line combinations. Figure 4 shows the five lines with the best fits out of the total of eleven lines studied. We can see that the fits to the lines in the 6122–6131 Å region are not as good as to the weaker lines used to find the model, but in view of the neglect of hyperfine splitting and the incorrect treatment of the magnetic splitting of these line, this is not too surprising. Our model does reproduce the qualitative feature of the spectral variations. The best model shows overabundances near both poles, with the highest abundance in the ring around the positive pole, as seen in Table 5. Note the similarity between this abundance model and that of Si, as well as with Fe, Nd and Pr.

Again we have computed a best uniform model and a solar model for Mn, with results reported in Table 5. Both (especially the uniform abundance model) appear to fit the modelled lines acceptably, but this is to a large extent an artifact of the fact that the Mn lines that we have modelled (and for which the χ^2/ν of the fit is computed) are relatively weak (typical equivalent widths of 40 mÅ or so). The solar model for these two lines is virtually a straight line at 1.00 (for solar abundance the lines have equivalent widths of only about 1–2 mÅ), but because the lines modelled are both weak and low resolution, even

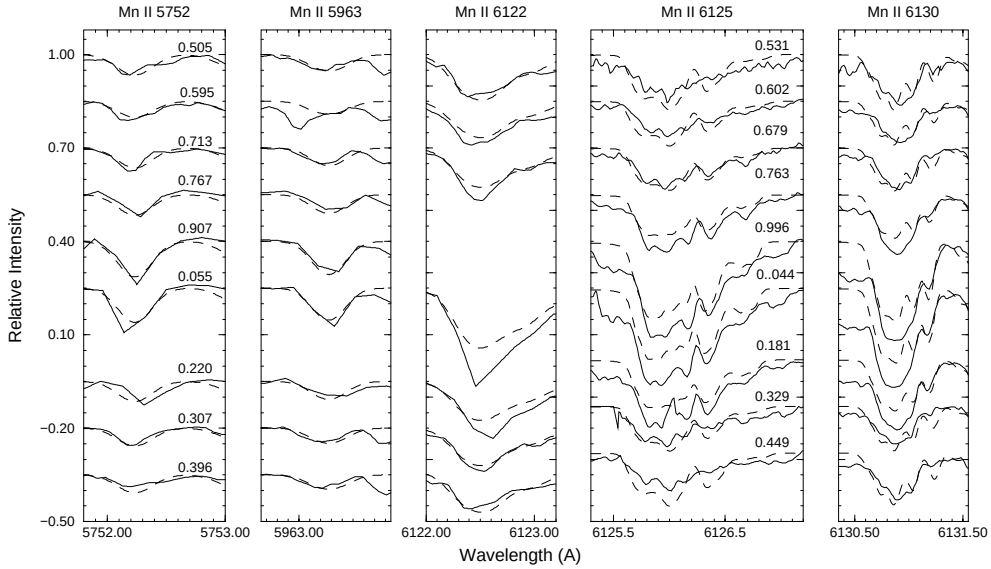

Fig. 4. A plot showing the three-ring fits to the observed profiles of five windows (12 lines of Mn II). Observations are shown as solid lines; model fits are dashed. Successive phases are separated by 0.15 in intensity (except between phase 0.055 and 0.220 for the first three boxes where the separation is 0.3). The phases are labeled inside the left-hand box and the fourth box. The three panels on the left are CASPEC spectra; the two on the right show CES data.

a model without lines does not give a really large value of χ^2/ν. If we had fit the model using the stronger lines at $\lambda\lambda$ 6120–6130 Å (for which Paschen-Back computations should be done), the solar abundance model would be very strongly excluded.

4.4. Iron distribution

In the case of iron, models with four and five rings gave very high abundances in the first ring, but again did not significantly improve the quality of the fit at all compared to the three-ring model. Therefore the adopted model is again a three ring model. The model was found by fitting the λ 6147 and λ 6149 lines simultaneously, and both of these lines are well fit. The adopted model is also consistent with the only marginal detection of two weak Fe I lines near λ 6136. The model fit is compared to CES data in Fig. 5.

Figure 6 shows a similar comparison for three lines in the CASPEC spectra. The line at λ 6175 is only in four of our CES spectra, and normalization close to the edge of the spectral range is subject to significant uncertainties, so the fit is not very good. We thus show the fit to that line in the CASPEC spectra; note however that the splitting was reproduced very nicely by the model in the four available CES spectra. The model iron distribution peaks at both poles at a value of about -3.2 and is almost one dex lower around the equator.

The comparison of the best uniform Fe abundance model, and a solar abundance model, with the observed spectra indicates that we cannot really exclude a uniform distribution of Fe, but that the typical abundance of Fe is almost one dex larger than solar. A solar abundance model provides a completely unacceptable fit to the data.

4.5. Praseodymium distribution

Pr III has strong hyperfine splitting that is not included in our modelling. This omission introduces some significant uncertainty into our results. We have only one strong, clean Pr line in the CES spectra, the Pr III line at λ 6160, first identified by Mathys & Cowley (1992). It is adjacent to a second Pr III line at λ 6161 which is heavily blended with lines of Cr II, Pr II and Fe II. Landé g-factors for the Pr III lines were supplied by Wyart (private communication). The $\log gf$-value for the Pr III lines were obtained from the Web database of Biémont et al. at `www.umh.ac.be/ astro/dream.shtml`; these data revise results reported by Palmeri et al. (2000). The Pr distribution found by our programme shows a decrease from -6.8 in the first ring to -9.3 in the second ring and then increases to about -5.5 at the positive pole. As with Si, the variations of χ^2/ν with the equatorial abundance show that the programme has selected an equatorial abundance for which the equator contributes nothing to the line; in fact for this ring we have only determined that the abundance is less than about -8.5. The model fit to the two lines is shown in Fig. 7.

There are a number of Pr II lines in the CES window, but most of them are expected to be quite weak. The line most likely to be detectable is the Pr II line at λ 6165, which is shown in Fig. 7. Although the strength of this line computed from our Pr III model is compatible with the observed spectra for phases away from the positive pole, when the line of sight sweeps over that pole the model derived from Pr III predicts a much stronger Pr II line than is observed. (This effect produces some of the excess depth in the red wing of the λ 6161 feature in Fig. 7 near phase 0.5.) Possibly this is due to errors in the atomic or stellar data data adopted, but if the effect is real,

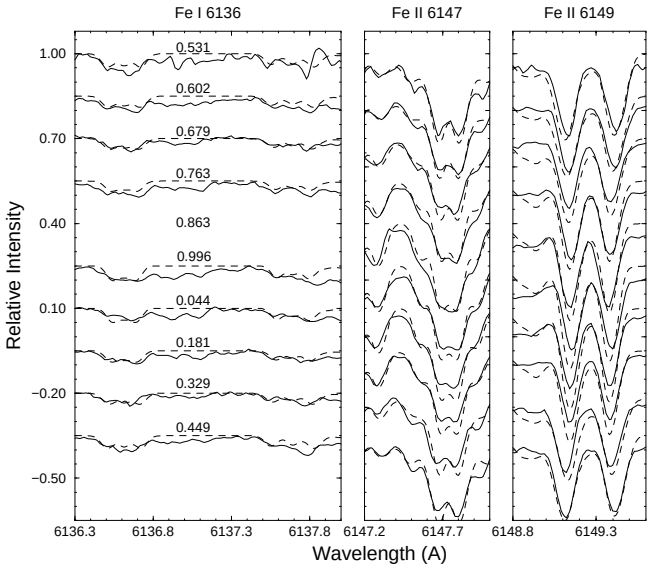

Fig. 5. A plot showing the three-ring fits to the observed profiles of four lines of Fe I and II. Observations are shown as solid lines; model fits are dashed. Successive phases are separated by 0.15 in intensity. The phases are labeled along the right border of the box. The λ 6149 line is the one used for the B_s observations from which the magnetic model was derived, so it is satisfying that a reasonable fit is obtained for this line.

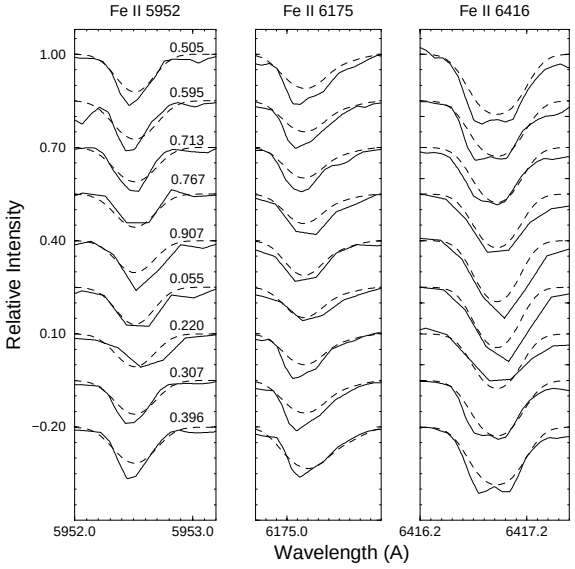

Fig. 6. A plot showing the three-ring fits to the observed profiles of three lines of Fe II in the CASPEC spectra. Observations are shown as solid lines; model fits are dashed. Successive phases are separated by 0.15 in intensity. The phases are labeled inside the left-hand box.

it may point to significant stratification of Pr in the stellar atmosphere.

The best fitting uniform abundance model does not fit the strong Pr III line at all well compared to the three-ring model, and the solar abundance fit may certainly be excluded. We consider that an abundance contrast of order two dex is confidently detected.

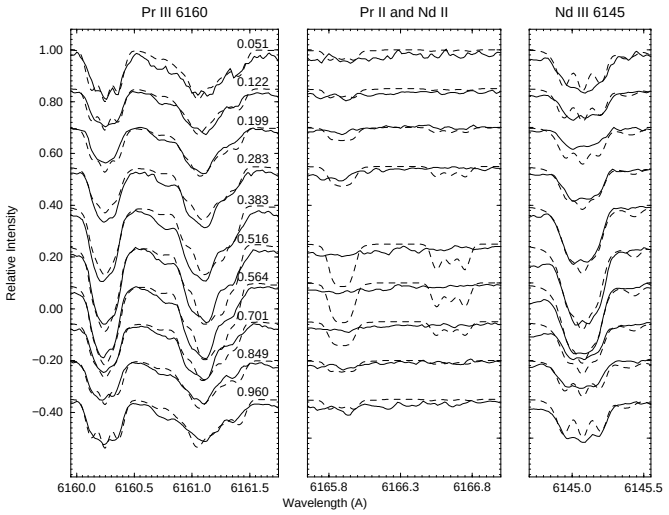

Fig. 7. A plot showing the three-ring fits to the observed profiles for the λ 6160–6161 lines of Pr III (left) and the λ 6145 line of Nd III (right). The middle panel illustrates the fact that models that fit Nd III and Pr III predict lines of Nd II and Pr II that are too strong at phases around 0.0; the two lines shown in this panel are Pr II 6165.9 and Nd II 6166.6. Observations are shown as solid lines; model fits are dashed. Successive phases are separated by 0.15 in intensity. The phases are labeled inside the left-hand box.

4.6. Neodymium distribution

Nd III, like Mn II and Pr III, is affected by strong hyperfine splitting. In addition, there are several stable isotopes of Nd, so isotope shifts contribute to the observed spectral line profiles. Neither effect is taken into account in our calculations, so our models will have some systematic errors because of this shortcoming. There is one strong Nd III line in the CES spectra at λ 6145. Theoretical Landé values obtained from Wyart (private communication) are listed in Table 3, and were used in our modelling. These Landé g values give a line of the correct width, but the π and σ components seem to be too bunched together, giving the computed line a more resolved structure than is observed; this may well be caused by the hyperfine splitting or isotope shifts.

A three ring model did as well as any model found in reproducing the line profile, with results that are satisfactory but not exact. Like the Fe distribution, Nd peaks at the poles, but much more strongly at the positive pole. The contrast between the second and third ring is quite large. Both the four and five ring models also showed this behaviour, which is needed to account for the rapid increase in equivalent width around phase 0.5. The best three ring model is shown in Fig. 7.

As a second example of cuts in the χ^2/ν surface which help to understand the uncertainties in our models, we show as open squares in the left panel of Fig. 2 the variations of χ^2/ν when the abundance $\log\epsilon_{\rm Nd}$(eq) on the equatorial ring is held constant at -10.50 (the solar value; but it could equally well have been held constant at -8.50) while the abundances on the two polar rings are

varied by $\Delta \log \epsilon$ around $\log \epsilon_{\rm Nd}({\rm neg\,pole}) = -6.50$ and $\log \epsilon_{\rm Nd}({\rm pos\,pole}) = -5.00$. As is the case with Si, decreasing the polar ring abundances by 0.8 dex is enough to produce an unacceptable model, and an increase of the two ring abundances by as much as 0.5 dex is not acceptable. In the right panel, the variations of χ^2/ν as the equatorial abundance is varied by $\Delta \log \epsilon$ from the model value of -9.00 is shown with open squares; in this cut, the abundances on the two polar rings are held constant at the values of the best fit of Table 5. As for Si and Pr, we find that the small equatorial abundance selected by the fitting programme really means simply that the contribution of the equatorial region to the line profile must be unimportant, and in fact any equatorial abundance of Nd less than about -8.0 is acceptable. Raising the equatorial abundance significantly above this value quickly produces an unacceptable model.

There are a number of good Nd II lines in the both the CASPEC and CES windows. We applied our model to these lines, and found a result similar to that already seen for Si and Pr. While none of the lines were fit well by our model, four lines (5804 Å, 5865 Å, 6133 Å, and 6166 Å) showed the same pattern. The computed model line strength goes from roughly correct at phase 0.5 to somewhat too deep around phase 0.0. We include the line at λ 6166.6 in Fig. 7 as an example. It appears that the Nd II distribution does not vary nearly as much with phase as the Nd III, although we must be a little cautious about this result because of the neglected hyperfine splitting and uncertain atomic data. Again, if the atomic data are correct, this result may point towards different vertical stratification through the atmosphere for singly and double ionized neodymium.

The best uniform abundance model provides a much worse fit to the data than our three-ring model (Table 5), and the solar abundance model can certainly be completely excluded.

4.7. Other elements

Using the CES spectra, we can provide some information about one element that is not obviously present. The strongest line of the O I triplet of lines at $\lambda\lambda$ 6155–58 is completely blended with overlapping strong lines of Cr II, but the two weaker components of this group are in an unblended region. It is not completely clear that these lines are present in the spectrum (they are always less than 5% deep), but there are suggestive weak depressions at the positions of both of the unblended components, in about the right relative strengths. Assuming that these lines are in fact present, we have derived a three-ring model which is tabulated in Table 5. The good χ^2/ν of the fit merely indicates that the lines are very weak. The deduced model requires O abundances which are everywhere below the solar value, by between about 0.5 and 1.5 dex, as is normal for magnetic Ap stars. If these weak depressions modelled are actually not the O I lines, these values may be taken as upper limits to the actual abundance of O. These lines are included in the right-most panel of Fig. 3.

5. Conclusions

In summary we find that with the CES data we were able to obtain models for Cr and Fe that account reasonably well for several spectral lines each, in spite of the draconian simplicity of the model used. We were also able to find distributions for Nd and Pr; however, these models rest essentially on only a single line each, and perhaps because of the the rather large abundance contrasts over the surface of the star of these elements, the models fits are not completely satisfactory. The fact that we do not treat the hyperfine splitting also introduces some uncertainty into these models. Using the low-resolution CASPEC data, we were also able to obtain reasonably consistent model distributions for Si and Mn, and were able to confirm the Fe model obtained with the CES data by modelling additional lines in the CASPEC spectra.

The models found are certainly fairly schematic: the magnetic field distribution is represented by a low-order expansion in co-linear multipoles, and the abundance distributions are approximated by three rings of uniform abundance, axisymmetric about the field axis and 60° in extent in magnetic latitude. However, even these rather simple models succeed in reproducing the main features of the observed intensity spectra, both the line shapes and their variations, so they appear to constitute a satisfactory first approximation. Because these models have very low resolution over the stellar surface, they certainly underestimate the local variations of magnetic field and abundance over the stellar surface. However, the models clearly establish that abundance variations of the order of a factor of ten are required to account for the observed variations of the Fe and Cr lines, while the extremely strong variations of Si, Mn, Nd and Pr lines suggest large-scale variations in surface abundance of these elements of factors as large as 10^3!

Each of the elements studied has a distinctive variation with magnetic colatitude. The elements Fe and Cr show less abundance variation over the surface than other elements studied. Fe is enhanced globally over the solar abundance by roughly one dex, with marginally higher abundances at both poles than at the equator. Cr has relatively uniform abundance enhancement of about two dex over most of the stellar surface, with a slightly stronger enhancement around the positive pole. The models for other elements studied all exhibit very large abundance contrasts. Si shows enhancements near the poles of the order of 1.5 dex relative to solar, strongly contrasting with the equatorial *depletion* by at least 1 dex. Mn shows the same general contrast as Si, but in this case the abundance at the equator is near solar, while the poles appear to have enhancements of about 2.5 dex. As with Cr and Si, the highest abundance occurs at the positive pole. Pr appears to be at least 4.5 dex overabundant relative to solar at the negative pole, dropping to 2 dex around the

equator and then rising to more than 6 dex at the positive pole. Nd is also extremely variable over the stellar surface; around the equator the abundance appears to be enhanced by not more than 2.5 dex from the solar value, but around the negative pole a typical enhancement of order 4 dex, and around the positive pole of 5.5 dex, occurs. Furthermore, there is some evidence from the Nd II lines that the distribution of Nd II and Nd III is not the same over the stellar surface, perhaps as a consequence of varying vertical stratification. Only the cosmically abundant element O is consistently underabundant with respect to solar abundances, and apparently fairly uniform over the stellar surface.

The common features for the overabundant elements are (1) that the lowest abundances are found around the magnetic equator, and (2) that the observed polar abundances are all considerably higher than solar. The polar abundances are highest at the slightly weaker positive pole in every case except Fe, where similar excesses are seen at both poles, perhaps representing saturation of the levitating mechanism. The naturally unabundant elements Mn, Pr and Nd show much larger enhancement factors, and much larger variations from one region to another, than the more abundant Cr and Fe, but the variations of Mn, Pr and Nd are roughly similar to those found for the still more abundant Si.

The very large abundance enhancements of most of the elements studied, (up to a factor of order 10^5 for Pr and Nd), and the extreme variations in abundance over the surface of the star of these elements, are unambiguous conclusions from even the rather schematic modelling carried out here. These results present some fairly serious challenges to theory. We look briefly at the extent to which our results may be understood in the light of available theoretical work.

Consider first the observed over- and underabundances relative to the sun. The general mild underabundance of O in HD 187474 is a natural consequence of diffusion; the weak radiative levitation (due to the high natural abundance) of this element (see e.g. Michaud et al. 1976; Gonzalez et al. 1995; Landstreet et al. 1998; Richer et al. 2000) means that the atmospheric abundance is expected to decline due to gravitational diffusion. Similarly, although there have been no detailed computations to our knowledge, the work of Michaud et al. (1976) certainly predicts that large overabundances of the rare earth elements should occur. This is in general agreement with our results for Pr and Nd. In contrast, the large overabundances of Si found around both poles, and the roughly 2 dex general overabundances of Cr and Mn, are not currently explained by diffusion; the most recent calculations for stars of $T_{\rm e} \approx 10\,000$ K (Richer et al. 2000) predict approximately solar abundance of Si and no more than 0.5 dex enhancement of Cr and Mn. (Although these computations are for non-magnetic stars, it is not obvious that the presence of a field will alter the results fundamentally, since the calculations include the effects of diffusion from far below the atmosphere, where the magnetic field will be energetically unimportant.)

Consider next the large surface inhomogeneities observed. Several mechanisms have been proposed for the development of such inhomogeneities. Mégessier (1984) considered the effects of horizontal diffusion of Si within the atmosphere driven by the oblique motions of ions in the magnetic field. Babel & Michaud (1991) have shown that in an oblique magnetic field, the anisotropy of magnetic desaturation leads to significant horizontal radiative forces, and hence to chemical migration. Babel (1992) has considered the possible effects of a magnetically controlled, inhomogeneous wind; assuming that a wind occurs near magnetic poles but is suppressed around the magnetic equator leads to different exterior boundary conditions and hence different accumulations of radiatively levitated material around the poles compared to the equator.

Models involving horizontal forces can only lead to important accumulations in the case where a limited amount of an element is brought into the atmosphere from below; if a particular element is continuously levitated into the atmosphere from below, the accretion from below will swamp the effects of horizontal motions because of the fact that the circumference of the star is far larger than the thickness of the atmosphere. It is not clear that any of the elements studied here have limited source reservoirs (especially considering that little is known about mixing below but near the stellar surface), so the relevance of horizontal forces is not clear. On the other hand, the inhomogeneous wind mechanism can affect surface abundances of any elements, but it is not known whether a stellar wind (well-mixed or separated) occurs on HD 187474, and so the relevance of this mechanism is also uncertain. However, if this wind mechanism does operate, it seems somewhat surprising that it leads to the largest accumulations where the elements that diffuse into the atmosphere can also escape. To conclude, we really have no specific theoretical predictions with which to compare; the production of clear predictions for some of the models noted above would make possible some very interesting comparisons.

Acknowledgements. We appreciate the telescope time awarded for this project by the European Southern Observatory, and the atomic data made available by the Vienna Atomic Line Database (VALD). We acknowledge helpful comments from the referee, J.-F. Donati. This work was supported in part by the Natural Sciences and Engineering Research Council of Canada.

References

Babcock, H. W. 1947, ApJ, 105, 105
Babcock, H. W. 1958, ApJS, 3, 141
Babel, J. 1992, A&A, 258, 449
Babel, J., & Michaud, G. 1991, A&A, 241, 493
Didelon, P. 1987, The Messenger, 49, 5
Glagolevskij, Y. V. 1994, Bull. Sp. Astrophys. Obs., 38, 152
Gonzalez, J.-F., Artru, M.-C., & Michaud, G. 1995, A&A, 302, 788

Grevesse, N., & Sauval, A. J. 1998, Sp. Sci. Rev., 85, 161
Hubrig, S., North, P., & Mathys, G. 2000, ApJ, 539, 352
Kupka, F., Piskunov, N. E., Ryabchikova, T. A., Stempels, H. C., & Weiss, W. W. 1999, A&AS, 138, 119
Landstreet, J. D. 1987, ApJ, 326, 967
Landstreet, J. D., Barker, P. K., Bohlender, D. A., & Jewison, M. S. 1988, ApJ, 344, 876
Landstreet, J. D., Dolez, N., & Vauclair, S. 1998, A&A, 333, 977
Landstreet, J. D., & Mathys, G. 2000, A&A, 359, 213
Leeman, S. 1964, Mon. Not. Astr. Soc. South Africa, 23, 6
Martin, G. A., Fuhr, J. R., & Wiese, W. L. 1988, Atomic Transition Probabilities, vol. 17, Suppl. 3
Martin, W. C., Zalubas, R., & Hagan, L. 1978, Atomic Energy Levels – The Rare Earth Elements
Mathys, G. 1991, A&AS, 89, 121
Mathys, G., & Cowley, C. R. 1992, A&A, 253, 199
Mathys, G., & Hubrig, S. 1997, A&AS, 124, 475
Mathys, G., Hubrig, S., Landstreet, J. D., Lanz, T., & Manfroid, J. 1997, A&AS, 123, 353
Mégessier, C. 1984, A&A, 138, 267
Michaud, G., Charland, Y., Vauclair, S., & Vauclair, G. 1976, ApJ, 210, 447
Moore, C. E. 1952, Atomic Energy Levels
Moore, C. E. 1959, A Multiplet Table of Astronomical Interest
Palmeri, P., Quinet, P., Frémat, Y., Wyart, J.-F., & Biémont, E. 2000, ApJS, 129, 367
Piskunov, N. E., Kupka, F., Ryabchikova, T. A., Weiss, W. W., & Jeffery, C. S. 1995, A&AS, 112, 525
Richer, J., Michaud, G., & Turcotte, S. 2000, ApJ, 529, 338
Ryabchikova, T. A., Piskunov, N. E., Stempels, H. C., Kupka, F., & Weiss, W. W. 1999, Proc. of the 6th International Colloquium on Atomic Spectra and Oscillator Strengths, Victoria BC, Canada, 1998, Phys. Scr., T83, 162
Wade, G. A., Bagnulo, S., Kochukov, O., Landstreet, J. D., Piskunov, N., & Stift, M. J. 2001, A&A, submitted